Available online at www.sciencedirect.com
ScienceDirect
Trans. Nonferrous Met. Soc. China 33(2023) 3003−3016
Transactions of Nonferrous Metals Society of China
www.tnmsc.cn

Fatigue crack propagation behavior in Ti−6Al−4V alloy with surface gradient structure fabricated by high-energy shot peening

Wen-guang ZHU, Chi MA, Cong-hui ZHANG, Kun HU, Xiang-kang ZENG

School of Metallurgical Engineering, Xi'an University of Architecture and Technology, Xi'an 710055, China

Received 5 April 2022; accepted 30 August 2022

Abstract: A gradient structure was successfully fabricated on the surface of Ti−6Al−4V alloy by high-energy shot peening (HESP), and its effect on fatigue crack propagation was investigated. Optical microscope, scanning electron microscope, transmission electron microscope and X-ray diffractometer were used to characterize the microstructure and residual stress evolution during HESP. The results show that a gradient nanostructure with residual compressive stress layer of 220 μm in depth is formed. The generation of gradient nanostructures improves the strength−ductility combination of the alloy. Maximum residual compressive stress is generated on the subsurface, which gradually increases with the increase of shot peening time. HESP treatment effectively reduces the crack propagation rate and increases the fatigue crack propagation life. The residual compressive stress reduces the effective stress intensity factor range ($\Delta K'_{\mathrm{eff}}$) at crack tip, thereby generating the crack closure effect and delaying the crack propagation. At the same time, the synergy effects of increase in grain boundaries, decrease in effective slip length and the plastic zone at the crack tip caused by the refinement of the surface grains can increase the crack propagation resistance as well.
Key words: Ti−6Al−4V alloy; high-energy shot peening; surface gradient structure; crack propagation rate

1 Introduction

Titanium alloys are widely used in aerospace, marine engineering and petrochemical fields due to high specific strength, excellent fatigue properties and outstanding corrosion resistance [1−3]. However, due to the intrinsic limited slip system in hcp structure, titanium alloy is prone to deform mainly along the base/prismatic plane which could not provide deformation along [0001] direction. During cyclic deformation process, cleavage facet along (0001) plane promotes the crack initiation, which finally results in early fracture and decreases the fatigue life [4]. These problems make challenges to the service safety of titanium alloy components.

In recent years, residual compressive stress and gradient nanostructures were generated at the surface, which significantly improved mechanical properties, especially fatigue strength of alloy [5]. Many typical modification methods such as high-energy shot peening (HESP) [6], laser shot peening (LSP) [7], ultrasonic surface rolling process (USRP) [8] and surface mechanical attrition treatment (SMAT) [9] were used to obtain surface gradient structure. Compared with other methods, HESP is commercially used in various industrial fields because of its convenient processing and higher efficiency. YANG et al [10] found that both residual compressive stress, fine-grained structure, high-density dislocations and work hardening effect introduced by shot peening were attributed to the improved strength−ductility combination in TC17. CHEN et al [11] studied the effect of shot peening on the fatigue properties of Ti_2AlNb alloys which found that increase in fatigue life is mainly due to the residual compressive stress and the reduction of

Corresponding author: Cong-hui ZHANG, Tel: +86-29-82202547, E-mail: zhangconghui@xauat.edu.cn
DOI: 10.1016/S1003-6326(23)66313-7
1003-6326/© 2023 The Nonferrous Metals Society of China. Published by Elsevier Ltd & Science Press

the notch stress concentration factor. However, to the author's knowledge, such researches mentioned above are mainly focused on the influence of shot peening on fatigue strength and its mechanism.

For fatigue crack propagation in titanium alloys, existing researches are mostly focused on bulk material. ZENG et al [12] pointed out that titanium alloy with lamellar structure has a lower crack growth rate, mainly due to tortuous crack propagation path and lower α/β phase interface stress. BIROSCA et al [13] believed that the crack propagation path of Ti-6246 alloy is strongly related to the crystal orientation of α grains. The crack tends to grow across lamellae favorably orientated for basal slip, while the crack path follows grains favorably orientated for prismatic slip in duplex microstructure. CHEN et al [14] studied the effect of α-phase morphology on fatigue crack propagation behavior of Ti−5Al−5Mo−5V−1Cr−1Fe alloy and found that samples with coarse secondary α-phase had better crack propagation resistance, which was mainly attributed to the obstruction of secondary α-phase to crack propagation. MA et al [15] considered that the orientation and temperature of the material are also important factors affecting the fatigue crack propagation behavior. Indeed, there are relatively few studies on the effect of surface gradient structure on the fatigue crack propagation behavior of alloys. WANG et al [16] studied the effect of shot peening on the fatigue short cracks of notched samples, and found that shot peening reduced the short crack propagation rate of Ti−6Al−4V titanium alloy, but increased the long crack propagation rate. PANT et al [17] found that after shot peening, the fatigue crack propagation rate of the sample decreased. But at the initial stage, the crack propagation rate of the sample after shot peening was higher. In general, the above research shows that the surface gradient structure could improve the fatigue crack propagation resistance in many conditions. However, the intrinsic mechanism of residual stress and microstructure on fatigue crack propagation behavior after shot peening needs to be further studied. There is still a lack of systematic research on the relationship and interaction mechanism between shot peening parameters−microstructure/residual stress−fatigue crack propagation behavior.

In this study, high-energy shot peening was used to prepare gradient structure on the surface of Ti−6Al−4V alloy. The microstructure and fatigue crack propagation properties of Ti−6Al−4V alloy were studied, and the effects of residual compressive stress and nano-gradient structure on the fatigue crack propagation were analyzed. This research could provide theoretical guidance for fatigue resistance manufacturing based on the surface modification in titanium alloys.

2 Experimental

The material employed in this study was a commercial rolled and annealed Ti−6Al−4V plate with a thickness of 3 mm. A schematic diagram of high-energy shot peening process is shown in Fig. 1, and the processing parameters are given in Table 1.

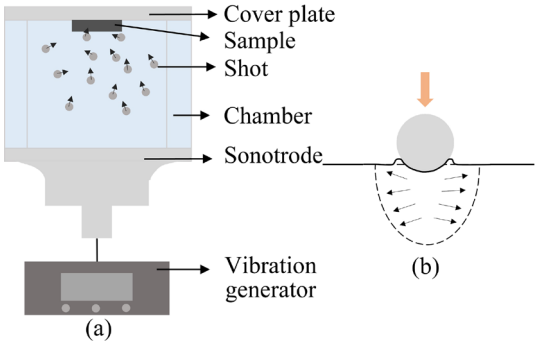

Fig. 1 Schematic diagram of shot peening: (a) Machining device of high-energy shot peening; (b) Deformation of material surface after shot peening impact

Table 1 HESP process parameters

Process parameter	Description or value
Shot peening material	Cast steel shot (ZG30)
Shot peening diameter/mm	0.3
Work pressure/MPa	0.4
Work time/min	15, 30, 45
Shot peening coverage/%	200
Shot peening method	Double-sided shot peening

The compact tension (CT) samples were designed according to GB/T 6398—2000, as shown in Fig. 2. The crack propagation experiment was carried out on the Instron 8801 fatigue machine. A 2 mm crack was prefabricated by the K-decreasing method. After prefabrication, a crack propagation experiment was carried out at room temperature. All fatigue tests were subjected to sinusoidal tension−tension loads with the maximum tensile stress of

1.7 kN, stress ratio of 0.1, and the frequency of 15 Hz. The COD gauge was used to monitor the crack length change during the crack propagation process.

Olympus GX51 metallurgical microscope was employed to observe the microstructure and the crack propagation path before and after shot peening. Electron backscatter diffraction technique (EBSD) was used to analyze the grain orientation and strain distribution. The EBSD sample was prepared by the electrolytic polishing method in an electrolyte of 10% perchloric acid and 90% methanol. The morphology of the Ti−6Al−4V alloy surface layer was characterized by JEM−2100 transmission electron microscope and Gemini SEM 300 scanning electron microscope. The TEM foils were mechanically ground to about 50 μm thick on metallographic sandpaper before discs of 3 mm in diameter were extracted. Finally, these foils were electrochemical polished at −20 to −30 °C in an electrolyte of 5% perchloric acid, 35% n-butyl alcohol and 60% methanol by MTP−1A twin jet electro-polisher at voltage of 30 V approximately. The D8 ADVANCE A25 X-ray diffractometer was used to measure the residual stress distribution. The scanning angle between 137° and 142° with the diffraction crystal plane (213) and the scanning speed of 0.2 (°)/min were selected.

3 Results

3.1 Surface gradient structure characterization of HESP alloy

Figure 3 shows the metallographic structure of

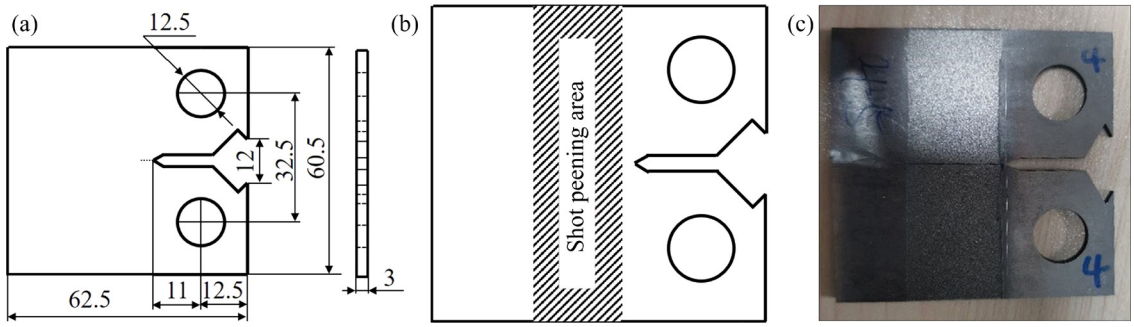

Fig. 2 Compact tension (CT) sample for fatigue crack growth rate test: (a) Schematic size of compact tension sample (mm); (b) Location of shot peening area on CT sample; (c) Sample after high-energy shot peening

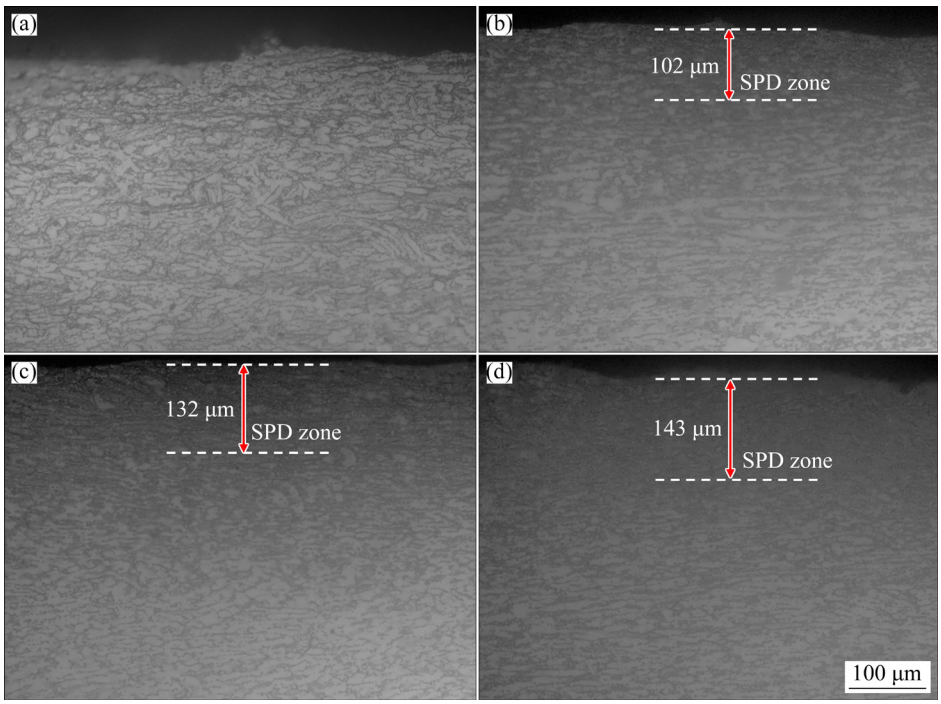

Fig. 3 Cross-section metallographic structures of Ti−6Al−4V alloy with different shot peening time: (a) BM (base metal); (b) HESP-15min; (c) HESP-30min; (d) HESP-45min

Ti−6Al−4V alloy with different shot peening durations. It is clearly seen that the original structure is a typical rolling and annealing structure with relatively uniform grain size, and the grains have not been fully recrystallized, showing an elongated equiaxed structure. Figures 3(b−d) show the microstructures after high-energy shot peening. Obviously, the surface layer displays a severe plastic deformation zone (SPD) with refined grains. With incremental shot peening time, the depth of the SPD zone gradually increases. It can be seen from Fig. 3 that the depth of the SPD zone increases from 102 to 132 μm as peening time increases from 15 to 30 min. However, when the shot peening time is increased from 30 to 45 min, the depth of the SPD zone only increases by 8.3%.

Figures 4(a, b) show the EBSD results of Ti−6Al−4V alloy before and after HESP treatment. The IPF image of as-received sample is shown in Fig. 4(a). It can be seen that the grains are relatively coarse and have random orientation. Figure 4(b) shows the microstructure of the HESP-30min sample. As shown in Fig. 4(b), due to the severe plastic deformation on the surface of the HESP treatment, the surface grains are not successfully calibrated by EBSD. Moreover, it can be observed that the grain size after the HESP treatment is significantly decreased, forming equiaxed grains. Figure 4(c, d) show kernel average misorientation (KAM) map of Ti−6Al−4V alloy before and after HESP treatment, which illustrates the degree of local deformation of the material. Figure 4(c) shows the KAM map of the original sample, and it can be observed that there is lower strain on the surface of the original sample. On the contrary, it is clearly seen from KAM map in Fig. 4(d) that the surface area undergoes severe plastic deformation after HESP treatment, and the strain intensity gradually

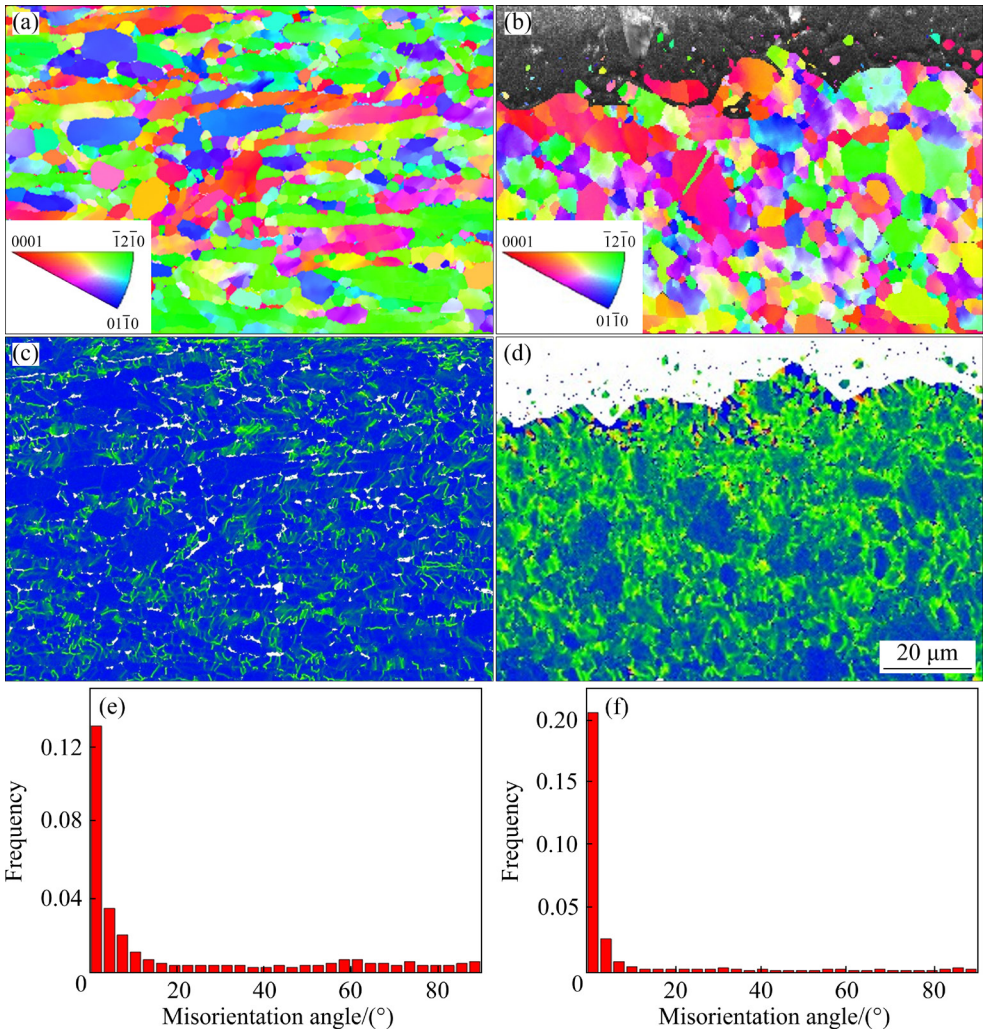

Fig. 4 IPF maps (a, b), KAM maps (c, d) and local misorientation distribution maps (e, f) of original sample (a, c, e) and HESP-30min sample (b, d, f)

decreases as the depth increases. The strain presents a gradient distribution. Figures 4(e, f) show the local misorientation distribution maps of Ti−6Al−4V alloy samples before and after HESP treatment. Compared with the original sample, the proportion of low-angle boundaries increases, and the proportion of high-angle boundaries decreases.

TEM characterization was used to analyze the degree of grain refinement at different depths from the surface of the samples after HESP treatment. Figure 5 shows the TEM images of the alloy after HESP treatment for 30 min.

During the shot peening process of Ti−6Al−4V, the strain gradually increases with the decrease of the depth from the shot peened surface [18]. At about 130 μm from the HESP-treated surface, neither the strain nor the strain rate is very large. It can be seen from Fig. 5(a) that the dislocation density inside the grain is high, and a large number of dislocation entanglements appear, which is caused by the simultaneous activation of multiple slip systems in the early stage of deformation [19]. In addition, the corresponding selected area electron diffraction (SAED) pattern shows periodic diffraction spots indexed as $\{11\bar{2}3\}$ zone axis, indicating that nanocrystals are not formed. The plastic deformation of α phase with hcp structure at room temperature occurs by the glide of dislocations along the prismatic and basal slip planes in the $\{11\bar{2}0\}$ slip directions [20]. Both the prismatic and basal slip systems have the same slip directions, which should promote cross slip between the prismatic and basal planes [21] and lead to a large number of dislocation entanglement (Fig. 5(a)), which is the characteristic of the materials with hcp structure such as CP-Ti [22] and pure Zr [23].

At about 80 μm from the HESP-treated surface, the strain and strain rate increase compared to those at about 130 μm from the surface. It can be seen

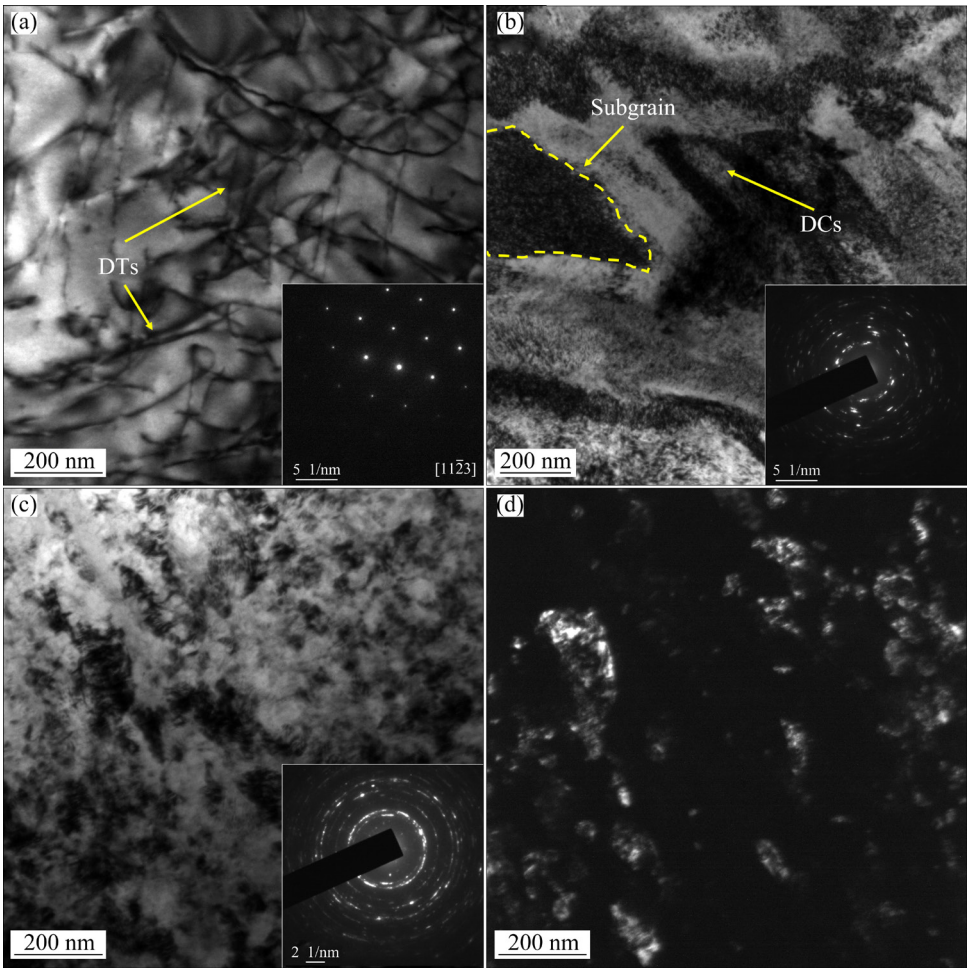

Fig. 5 TEM images of surface gradient structure of HESP-30min sample: (a−c) Bright field images at 130, 80 and 0 μm from topmost surface; (d) Dark field image of (c) (DTs and DCs represent dislocation tangles and dislocation cells, respectively)

from Fig. 5(b) that the dislocation density here is much higher than that in Fig. 5(a), and a number of dislocation cell and subgrain are produced. This is mainly because when the strain and strain rate increase, in order to reduce the energy of system, a large number of dislocation entanglements and dislocation band boundaries continuously absorb and annihilate dislocations, so that the orientation among the grains gradually increases, and the original coarse grains are gradually refined [24,25]. In addition, the corresponding SAED pattern is approximately circular, which indicates that in the subsurface layer about 80 μm from the surface, the original coarse grains are refined, resulting in nanoscale subgrains with random orientations.

Figures 5(c, d) show the TEM bright-field images and dark-field images of the topmost layer after HESP treatment, respectively, where the maximum strain and strain rate are present, and the degree of plastic deformation is very severe. It can be seen from Fig. 5(c) that the nanoscale sub-grains are further refined into uniform equiaxed nanocrystals. The corresponding SAED patterns are annularly distributed, which further proves that the coarse grains in the topmost layer of the material are refined into nanocrystals with random orientations. LIU and LI [26] found that when studying the surface nanocrystallization mechanism of α phase in Ti−6Al−4V treated by high-energy shot peening, under large strain and high strain rate, the transformation of α equiaxed ultrafine grains into equiaxed nanocrystals does not undergo a series of nucleation and growth, but undergoes dynamic recrystallization through subgrain rotation. In other words, the subgrains absorb slip dislocations continuously, which makes the orientation difference between adjacent subgrains increase continuously. Subgrain rotation is a common phenomenon in close-packed hexagonal α phase during shot peening of TC4 alloy, which is the main mechanism for the transformation of close-packed hexagonal α equiaxed ultrafine grains into equiaxed nanocrystals.

By considering the results of EBSD analysis and TEM characterization, it is clearly displayed that gradient nano-structure is formed on the surface of Ti−6Al−4V alloy after HESP treatment. This result has been confirmed by the previous study of high-energy shot peening of Ti−6Al−4V alloy with bi-modal and lamellar structure [6].

3.2 Residual stress distribution in surface gradient layer

It is well known that the HESP treatment results in grain refinement, high density dislocations and work hardening, as well as deep residual compressive stresses on the material surface [27]. Figure 6 shows the distribution of residual stress along the depth direction at different shot peening time. The results manifest that the depth of residual compressive stress layer is about 220 μm and the maximum residual compressive stress increases with the increase of shot peening time. In HESP-45min sample, the residual compressive stress at the topmost surface is 797 MPa, and the maximum residual compressive stress is 884 MPa on the subsurface.

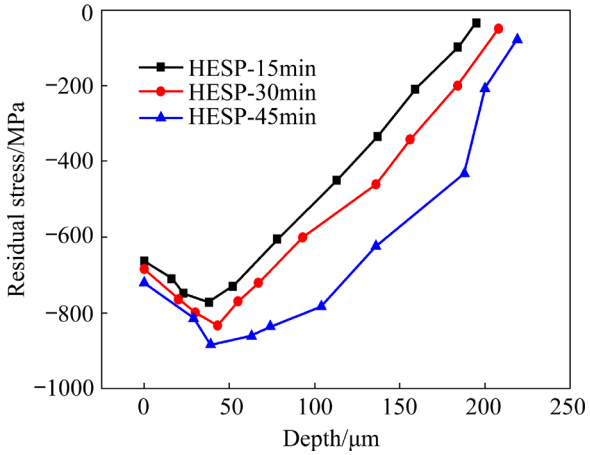

Fig. 6 Residual stress along depth direction of Ti−6Al−4V alloy with different shot peening time: (a) HESP-15min; (b) HESP-30min; (c) HESP-45min

As shown in Fig. 6, the residual compressive stress shows the tendency of increasing to maximum first and then decreasing with incremental depth. The reason for this trend may be due to the energy transfer in the process of HESP. During shot peening, the surface of the material undergoes severe plastic deformation, and the kinetic energy of the shot peening is converted into plastic distortion energy and stored in the material. However, due to the weak surface constraint, part of the energy is released on the free surface, which slightly reduces the residual compressive stress on the surface. Subsequently, when the energy is transferred to the subsurface, more energy can be stored in the grain internal due to the strong constraints of interior materials, thus introducing higher residual compressive stress. In the deeper

region, because only part of the energy can be reached, the shot peening energy gradually decays with the increase of depth, which leads to the residual compressive stress gradually decreasing with the increase of depth [28].

3.3 Fatigue crack propagation behavior of HESP alloy

3.3.1 Crack propagation rate analysis

The crack propagation is closely related to the cycle of loading. Figure 7(a) shows the relationship between crack length a and cycle number N of sample with different shot peening time. As can be seen from Fig. 7 that, for Ti−6Al−4V alloy treated with different shot peening time, the crack length gradually increases with the increase of the cycle number. Meanwhile, the slope of the curve gradually increases, indicating that the growth rate of crack length is accelerated. Figure 7(b) shows the fatigue crack life of Ti−6Al−4V alloy with different shot peening time. It can be seen that the fatigue life of untreated sample is 69701, while the fatigue life after shot peening for 15, 30 and 45 min is 115573, 124965 and 105187, respectively. Compared with untreated sample, the cycle number is increased by 62.2%, 78.9% and 52.6%, respectively. The fatigue life of HESP-45min sample is lower than that of other treated samples, which is mainly attributed to the increase of material surface roughness and defects caused by excessive shot peening.

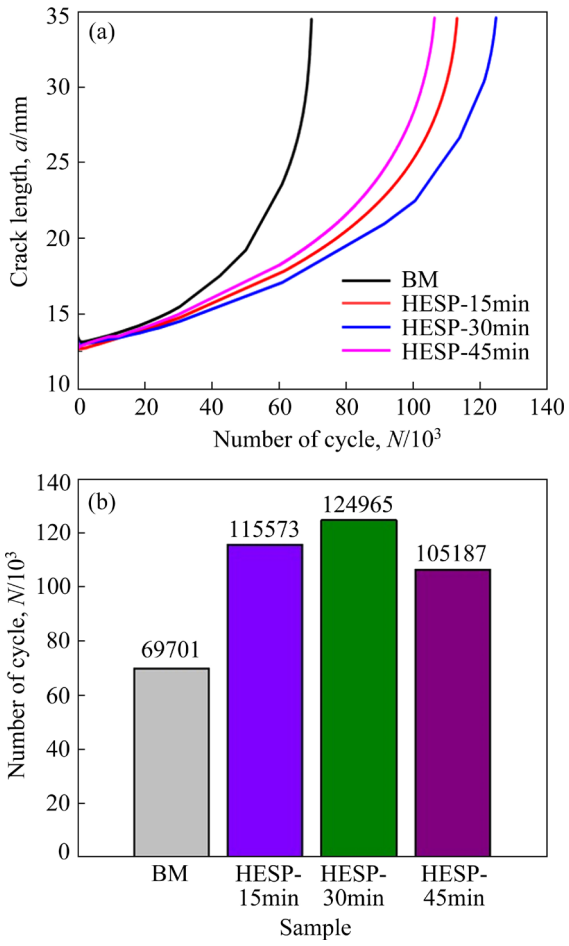

Fig. 7 Crack length−cycle number curves (a) and fatigue crack lives (b) of Ti−6Al−4V alloy with different shot peening time (BM−Base metal)

In order to study the effect of shot peening duration on crack propagation rate, the relationship between crack propagation rate (da/dN) and stress intensity factor range (ΔK) was employed to analyze the stable crack propagation stage. Stress intensity factor can be written as

$$\Delta K = \frac{\Delta P}{B\sqrt{W}} \cdot Y \tag{1}$$

where ΔP is external constant load ($\Delta P = P_{max} - P_{min}$), B is the thickness of the sample, W is the width of the sample, and Y is the shape factor.

$$Y = \frac{2 + a/w}{(1 + a/w)(1 + a/w)^{3/2}} \cdot [0.886 + 4.64(a/w) - 13.32(a/w)^2 + 14.42(a/w)^3 - 5.60(a/w)^4] \tag{2}$$

According to Paris formula [29], the relationship between da/dN and ΔK during cyclic loading can be given by Eq. (3):

$$\frac{da}{dN} = C(\Delta K)^m \tag{3}$$

where C and m are constants that are depended on the material, environment and stress ratio. In Eq. (3), C is the intercept of da/dN−ΔK curve, and m is the slope of da/dN−ΔK curve, implying the growth speed of crack propagation rate, which can reflect the anti-crack propagation ability through its change.

Figure 8 shows the relationship between crack propagation rate (da/dN) and stress intensity factor range (ΔK) with different shot peening time fitted by Paris formula. As shown in Fig. 8, under the double logarithmic coordinates, linear correlation between da/dN and ΔK is displayed. Compared with the untreated sample, the da/dN−ΔK curve of the shot-peened sample shows a downward trend, which indicates that shot peening reduces the crack propagation rate at the same ΔK. When ΔK >35 MPa·m$^{1/2}$, the samples treated by shot

peening fracture at almost the same crack propagation rate. The fitting values of C and m are summarized in Table 2. Obviously, C value increases from 1.58×10^{-9} to 7.94×10^{-8}, 9.77×10^{-8} and 1.05×10^{-8}, while m decreases from 3.32 to 2.74, 2.72 and 2.65 in the untreated sample, HESP-15min, HESP-30min and HESP-45min samples, respectively. These changes indicate that the crack propagation rate under the same ΔK would decrease after HESP. SUN et al [30] found similar results in laser peening Ti-17 alloy.

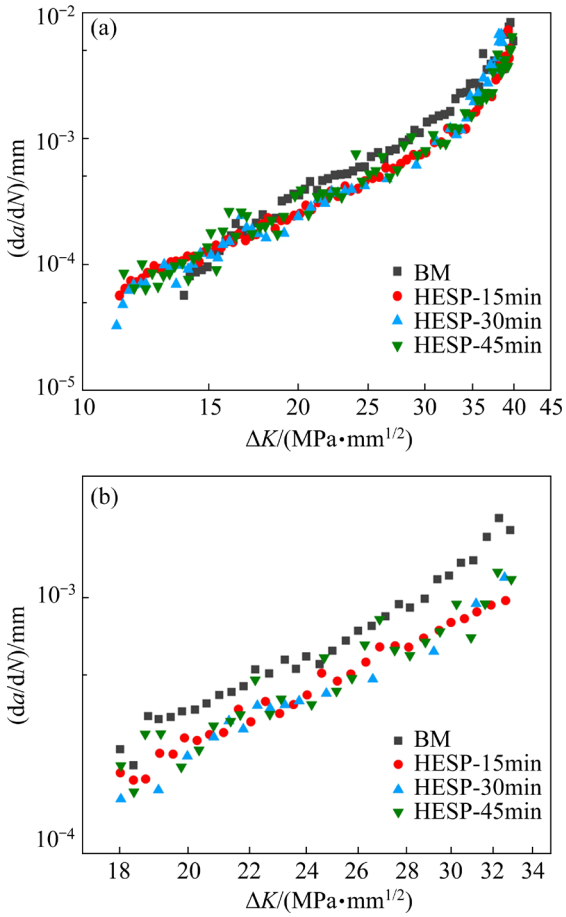

Fig. 8 Relationship between crack propagation rate of Ti−6Al−4V alloy and stress intensity factor range with different shot peening time: (a) Whole stage of crack propagation; (b) Stable stage of crack propagation

Table 2 Material constants, C and m, of untreated and shot-peened samples

Sample	C	m	R^2
Untreated	1.58×10^{-9}	3.32	0.976
HESP-15min	7.94×10^{-8}	2.74	0.997
HESP-30min	9.77×10^{-8}	2.72	0.997
HESP-45min	1.05×10^{-8}	2.65	0.997

At lower ΔK, the residual compressive stress introduced by shot peening decreases the effective load, thus reducing the driving force of fatigue crack propagation and hindering crack propagation. Generally speaking, the longer the shot peening time is, the greater the residual compressive stress is introduced on the surface of the material, thereby reducing the driving force for fatigue crack propagation to a greater extent. However, with the extension of shot peening time, the surface quality of the material deteriorates, which can accelerate the fatigue crack propagation of the material [31]. The degradation of surface quality caused by long shot peening time is also one of the reasons why the fatigue crack propagation rate of HESP-45min sample is higher than that of HESP-30min and HESP-15min samples.

3.3.2 Tortuosity of crack propagation path

Fatigue crack propagation path is mainly along a certain direction with the lowest energy. Meanwhile, some phenomena such as deflection, bifurcation and blunting may occur in the process of propagation. Figures 9(a_1, b_1) and 9(a_2, b_2) show the propagation paths of the original sample and the HESP-30min sample at the initial stage of crack propagation (Zone A: ΔK<18 MPa·mm$^{1/2}$), respectively. Compared with the original sample, the crack propagation path after HESP treatment is more tortuous. Meanwhile, deflection, secondary cracks and microcracks can be clearly observed in the crack propagation path of HESP treated samples.

Figures 9(c_1, d_1) and 9(c_2, d_2) show the crack propagation behavior at Zone B (18 MPa·mm$^{1/2}$ < ΔK < 34 MPa·mm$^{1/2}$) of the original sample and the HESP-30min sample, respectively. Similar to that observed in Zone A, it is clearly seen that the crack propagation path of the original sample is still relatively flat. However, a more tortuous crack with few secondary cracks can be observed on the propagation path of the HESP-30min sample. Generally speaking, there is a positive correlation between the tortuosity of the crack propagation path and the crack resistance of the material. The more torturous the propagation path is, the more effective the crack resistance is. In general, high-energy shot peening can obviously reduce the crack growth rate at the initial stage of crack growth, and with the increase of crack length, the retarding effect weakens gradually.

3.3.3 Fractograph of CT samples after crack propagation test

The fracture morphologies in the different stages of Ti−6Al−4V alloy before and after HESP treatment are illustrated in Fig. 10. Tearing ridges, river patterns and cleavage facets are clearly observed, which indicates that cleavage fracture is the main fracture mode of Ti−6Al−4V alloy under fatigue load. Figures 10(a_2, b_2) show the fracture morphologies of HESP-30min sample at the initial stage of crack propagation (Zone A). Compared with the original sample as shown in Figs. 10(a_1, b_1), the fracture is rougher with more cleavage steps, which indicates that crack propagation path after

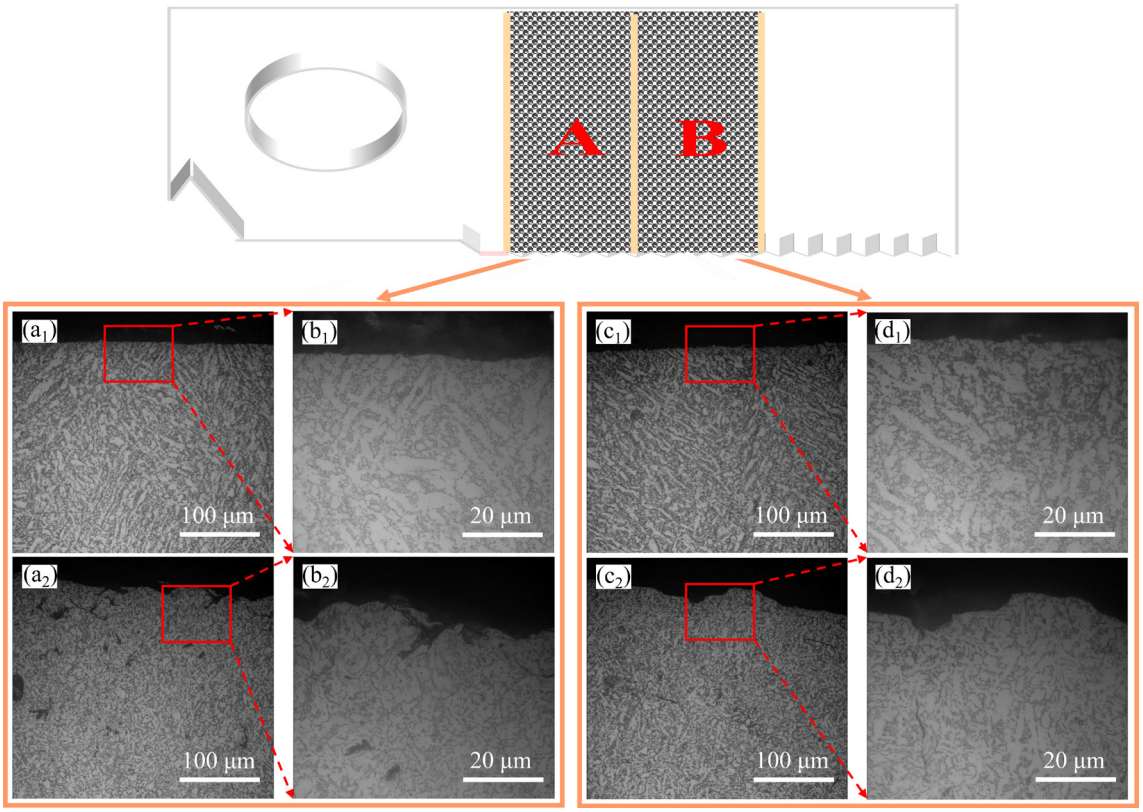

Fig. 9 Crack propagation path: (a_1−d_1) Original sample; (a_2−d_2) HESP-30min sample

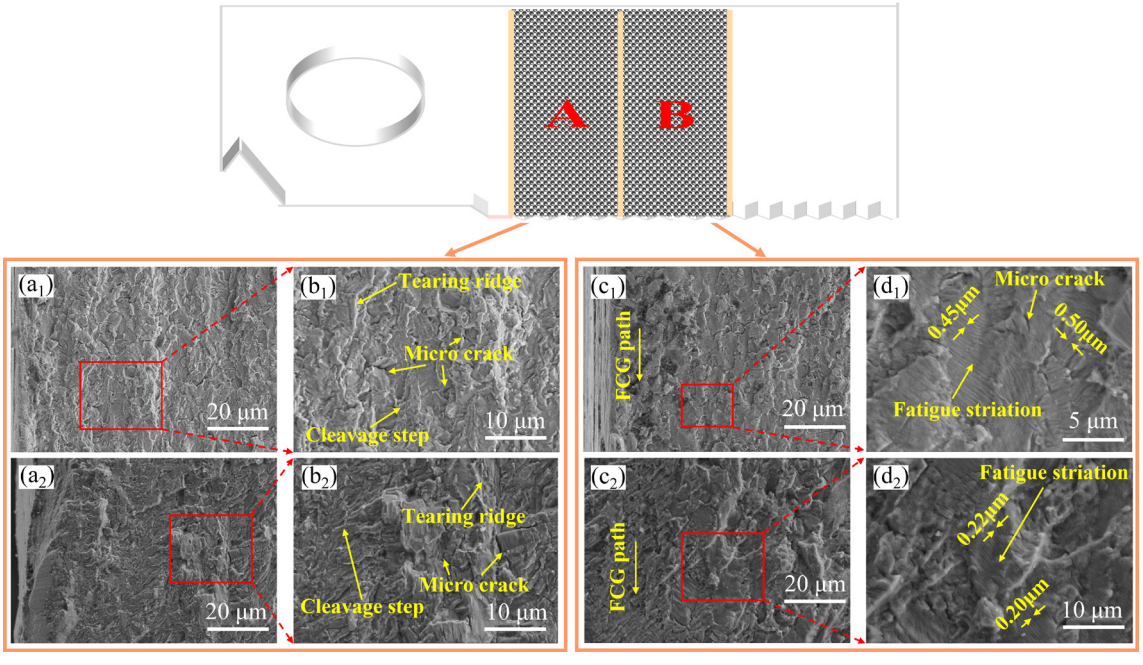

Fig. 10 Fracture morphologies: (a_1−d_1) Original sample; (a_2−d_2) HESP-30min sample

shot peening is tortuous and more energy is consumed in the process of crack propagation. By studying the effect of grain size on fatigue crack propagation of titanium alloy, YODER et al [32] found that the average effective grain size has an crucial effect on fatigue crack propagation. The larger the grain size is, the fewer the grain boundaries are, and the weaker the hindrance to crack propagation is. High-energy shot peening refines the surface grain effectively and increases the number of grain boundary dramatically. Thus, more energy is needed for crack propagation through the grain boundary.

A large number of fatigue striations as shown in Figs. 10(c_2, d_2) can be observed when the crack propagates to Zone B. Fatigue striations are produced by microscopic plastic deformation during cyclic loading. The crack propagation rate can be expressed by fatigue striations spacing. As shown in Figs. 10(d_1, d_2), compared with the original sample, the average spacing of fatigue striations on the fracture surface of HESP sample decreases from 0.45 to 0.22 μm, which illustrates that the crack propagation rate of Ti−6Al−4V alloy is obviously reduced after high-energy shot peening.

4 Discussion

After high-energy shot peening treatment, the crack propagation rate of Ti−6Al−4V alloy decreases obviously compared with the original sample, which is mainly depended on two factors. Firstly, the crack closure effect is caused by the residual compressive stress [33]; Secondly, the gradient structure introduced by high-energy shot peening on the surface improves the strength of the material. The higher strength reduces plastic zone size and delays fatigue crack propagation [34]. In addition, the gradient structure is regarded as one of the heterostructures, and its unique back stress strain hardening improves the ductility of the material [35]. Generally speaking, materials with good ductility can delay the initiation and propagation of cracks.

4.1 Effect of residual compressive stress on crack propagation

The residual compressive stress introduced on the material surface by high-energy shot peening has long been considered to be one of the important reasons for the improvement of material fatigue properties. SUN et al [36] studied the effect of the residual stress on the fatigue life of the laser shock peened Ti-17 alloy, and pointed out that the crack closure effect caused by residual stress played an important role in delaying the fatigue crack propagation of Ti-17 alloy. AGUADO-MONTERO et al [37] analyzed the fatigue behavior of plain fatigue specimens and notch fatigue specimens and found that the fatigue improvement due to shot peening is depended to a great extent upon the in-depth compressive residual stress profile produced in the specimen. In this section, the process of crack closure effect caused by residual compressive stress and the mechanism of crack closure effect delaying fatigue crack propagation are described in detail.

ELBER [38] believes that the crack can only propagate where the crack surface is completely separated. Herein, the effective stress range (ΔP_{eff}) and the corresponding effective stress intensity factor range (ΔK_{eff}) are introduced to illustrate the effect of residual compressive stress on crack closure. Combined with Eq. (1), the ΔK_{eff} can be expressed as follows:

$$\Delta K_{\text{eff}} = \frac{\Delta P_{\text{eff}}}{B\sqrt{W}} Y = \frac{P_{\max} - P_{\text{op}}}{B\sqrt{W}} Y \tag{4}$$

where $P_{\max}$ is the maximum stress of applied load, and P_{op} is the crack opening load. It can be clearly seen from Fig. 11(a) that during the fatigue loading process, the far-field load is ($P_{\max}$–$P_{\min}$), while the actual load at the crack tip is ($P_{\max}$–P_{op}). In the process of fatigue loading, the crack surfaces are gradually separated until the crack is fully opened when the external load reaches P_{op}. In other words, when $P_{\min} < P < P_{\text{op}}$, the crack is closed.

After high-energy shot peening, the residual compressive stress (P_{crs}) is introduced at the crack tip which changes the actual stress state of the crack tip, as shown in Fig. 11(b). The effective stress intensity factor range ($\Delta K'_{\text{eff}}$) under the combined action of external load and residual compressive stress can be expressed by Eq. (5):

$$\Delta K'_{\text{eff}} = \frac{\Delta P'_{\text{eff}}}{B\sqrt{W}} Y = \frac{P_{\max} - P_{\text{op}} - P_{\text{crs}}}{B\sqrt{W}} Y \tag{5}$$

where $\Delta P'_{\text{eff}}$ is the effective external load after high-energy shot peening. It can be seen from

Eq. (5) that the introduced compressive residual stress reduces the effective applied load and the overall stress intensity factor, which reduces the effective stress intensity factor range $\Delta K'_{\mathrm{eff}}$, leading to crack closure effect and delaying the crack propagation rate.

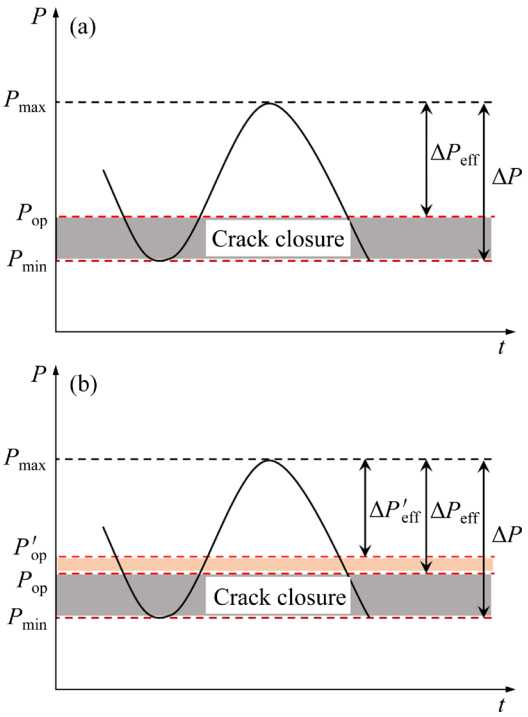

Fig. 11 Schematic diagram of crack closure effect under constant amplitude loading: (a) Original sample; (b) Shot-peened sample

4.2 Influence of surface gradient structure on crack propagation

In the process of fatigue crack propagation, plastic deformation occurs at the crack tip [39], which results in a butterfly-shaped plastic deformation zone, as shown in Figs. 12(a, b). The size of the plastic zone directly affects the speed of fatigue crack propagation. In Mode I (tensile opening fracture), the plastic zone size (r_{p}) can be given by Eq. (6):

$$r_{\mathrm{p}} = \frac{1}{\pi}\left(\frac{\Delta K}{\sigma'_{\mathrm{y}}}\right)^2 \tag{6}$$

where σ'_{y} is the yield strength at the 0.2% strain of the cyclic stress−strain curve, which is called cyclic yield strength. Generally speaking, σ'_{y} increases with the increase of monotonic yield strength (σ_{y}). Therefore, for σ'_{y}, in the absence of this parameter, σ_{y} is usually used instead [40].

According to Eq. (6), the variation of the plastic zone size of the original sample and HESP-30min sample with the increase of the crack length is estimated, as shown in Fig. 12(c). It can be seen that high-energy shot peening reduces the plastic zone size at fatigue crack tip, which is mainly due to the decrease of ΔK (caused by the residual compressive stress on the surface of the material) and the increase of σ'_{y} (caused by grain refinement). OULD et al [41] pointed out that the fatigue crack propagation rate is a function of the plastic zone size is. In this function, the larger the plastic zone size is, the larger the fatigue crack propagation rate is. A functional relationship between fatigue crack propagation rate and plastic zone size is given in Eq. (7):

$$\frac{\mathrm{d}a}{\mathrm{d}N} = A \cdot r_{\mathrm{p}}^2 \tag{7}$$

where A is correction factor of the plastic zone. In addition, a large number of grain boundaries produced by grain refinement on the surface of Ti−6Al−4V alloy directly hinder the fatigue crack propagation. Meanwhile, grain refinement increases σ'_{y} of the material. Under the combined influence of σ'_{y} and ΔK, the size of the plastic zone at the

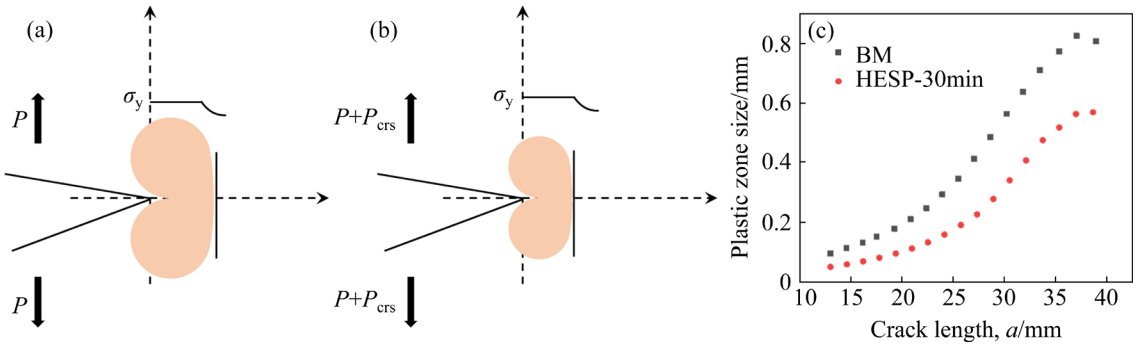

Fig. 12 Plastic zone size: (a, b) Schematic; (c) Calculated result

tip of the fatigue crack of the HESP specimen decreases, and the fatigue crack propagation rate also decreases accordingly.

Furthermore, the gradient structure is regarded as one of the heterostructures. When heterostructure metal materials are deformed, the strain is inhomogeneous but continuous, which can lead to strain gradients in the material, resulting in geometrically necessary dislocations (GNDs) to accommodate this strain gradients [35]. On the one hand, the generation of GNDs increases the dislocation density, which is favorable for dislocation forest hardening. On the other hand, in order to accommodate the plastic incompatibility between adjacent layers of the gradient structure, GNDs accumulate at the boundary of each adjacent layer, resulting in a large back stress [42]. Back stress can not only increase the yield strength, but also significantly enhance the strain hardening effect, thereby achieving the purpose of improving ductility [43]. In common homogeneous structural metals, the dislocation forest hardening is the dominant hardening mechanism due to the small back stress. However, for heterostructure metal materials, the back stress hardening must be considered, and sometimes even exceeds the effect of dislocation forest hardening [44].

In this study, a gradient structure layer is formed under the surface after high-energy shot peening of Ti−6Al−4V alloy. Since the surface of Ti−6Al−4V alloy undergoes severe plastic deformation during high-energy shot peening, many dislocations are generated in the gradient structure layer (as shown in Fig. 5(a)), resulting in dislocation hardening effect, so that the strength of the material is improved. In addition, the back stress generated in the gradient structure can not only increase the yield strength but also significantly enhance the strain hardening to increase the ductility [35]. In Ref. [44], the strength and ductility of Ti−6Al−4V alloy were improved after high-energy shot peening as well, which was attributed to the synergistic effect of dislocation forest hardening and back stress strain hardening. The gradient structure formed on the surface of Ti−6Al−4V alloy after high-energy shot peening enables the material to have better strength−elongation combination, thereby significantly improving fatigue properties and delaying fatigue crack propagation [45].

5 Conclusions

(1) After HESP treatment, a surface gradient nanostructure with residual compressive stress layer is successfully fabricated. The residual compressive stress gradually increases with the increase of shot peening time.

(2) The HESP significantly increases the fatigue crack propagation life compared with the untreated sample.

(3) Both crack closure effect caused by residual compressive stress and plastic zone size decrease, and back stress strain hardening caused by the surface gradient microstructure is the origin of the improved fatigue crack propagation resistance.

Acknowledgments

This work was supported by the National Natural Science Foundation of China (No. 51674187), the International Joint Research Center for Value-added Metallurgy and Processing of Non-ferrous Metals, China (No. 2019SD0010), and the Key Industry Chain (Group)-Industrial Field in Shaanxi Province, China (No. 2019ZDLGY05-03).

References

[1] CUI Chun-xiang, HU Bao-min, ZHAO Li-chen, LIU Shuang-jin. Titanium alloy production technology, market prospects and industry development [J]. Materials & Design, 2011, 32: 1684−1691.

[2] BOYER R R. An overview on the use of titanium in the aerospace industry [J]. Materials Science and Engineering A, 1996, 213: 103−114.

[3] MARTINEZ A L, FLAMINI D O, SAIDMAN S B. Corrosion resistance improvement of Ti−6Al−4V alloy by anodization in the presence of inhibitor ions [J]. Transactions of Nonferrous Metals Society of China, 2022, 32: 1896−1909.

[4] ZHANG Xiao-hua, LIU Dao-xin. Effect of shot peening on fretting fatigue of Ti811 alloy at elevated temperature [J]. International Journal of Fatigue, 2009, 31: 889−893.

[5] GAO Xing-ke, LI Bo-chuan, JIANG Chao. The critical assessment for the fatigue limit of nanocrystallized surface with micro-notches obtained by ultrasonic surface rolling processing [J]. International Journal of Fatigue, 2021, 143: 105988.

[6] ZHANG Cong-hui, HU Kun, ZHENG Min, ZHU Wen-guang, SONG Guo-dong. Effect of surface nanocrystallization on fatigue properties of Ti−6Al−4V alloys with bimodal and lamellar structure [J]. Materials Science and Engineering A, 2021, 813: 141142.

[7] CHEN Lan, REN Xu-dong, ZHOU Wang-fan, TONG Zhao-peng, ADU-GYAMFI S, YE Yun-xia, REN Yun-peng.

Evolution of microstructure and grain refinement mechanism of pure nickel induced by laser shock peening [J]. Materials Science and Engineering A, 2018, 728: 20−29.

[8] LUAN Xiao-sheng, ZHAO Wen-xiang, LIANG Zhi-qiang, XIAO Shi-hong, LIANG Guo-xiang, CHEN Yi-fan, ZOU Shi-kun, WANG Xi-bin. Experimental study on surface integrity of ultra-high-strength steel by ultrasonic hot rolling surface strengthening [J]. Surface and Coatings Technology, 2020: 392.

[9] BAHL S, SUWAS S, UNGÀR T, CHATTERJEE K. Elucidating microstructural evolution and strengthening mechanisms in nanocrystalline surface induced by surface mechanical attrition treatment of stainless steel [J]. Acta Materialia, 2017, 122: 138−151.

[10] YANG C, LIU Y G, SHI Y H, LI M Q. Microstructure characterization and tensile properties of processed TC17 via high energy shot peening [J]. Materials Science and Engineering A, 2020, 784: 139298.

[11] CHEN Y X, WANG J C, GAO Y K, FENG A H. Effect of shot peening on fatigue performance of Ti_2AlNb intermetallic alloy [J]. International Journal of Fatigue, 2019, 127: 53−57.

[12] SHI Xiao-hui, ZENG Wei-dong, SHI Chun-ling, WANG Hao-jun, JIA Zhi-qiang. The effects of colony microstructure on the fatigue crack growth behavior for Ti−6A1−2Zr−2Sn−3Mo−1Cr−2Nb titanium alloy [J]. Materials Science and Engineering A, 2015, 621: 252−258.

[13] BIROSCA S, BUFFIERE J Y, KARADGE M, PREUSS M. 3-D observations of short fatigue crack interaction with lamellar and duplex microstructures in a two-phase titanium alloy [J]. Acta Materialia, 2011, 59: 1510−1522.

[14] CHEN Kui-wai, PAN Su-ping, LIU Hui-qun, JIANG Yong. Effect of α phase morphology on fatigue crack growth behavior of Ti−5Al−5Mo−5V−1Cr−1Fe alloy [J]. Transactions of Nonferrous Metals Society of China, 2020, 30: 2459−2471.

[15] MA X F, ZHAI H L, ZUO L, ZHANG W J, RUI S S, HAN Q N, JIANG J S, LI C P, CHEN G F, QIAN G A, ZHAO S J. Fatigue short crack propagation behavior of selective laser melted Inconel 718 alloy by in-situ SEM study: Influence of orientation and temperature [J]. International Journal of Fatigue, 2020, 139: 105739.

[16] WANG Yan-zhong, ZHANG Ya-ping, SONG Guan-hua, NIU Wen-tao, XU Zi-chun, HUANG Chang-xu. Effect of shot peening on fatigue crack propagation of Ti6Al4V [J]. Materials Today Communications, 2020, 25: 101430.

[17] PANT B K, PAVAN A H V, PRAKASH R V, KAMARAJ M. Effect of laser peening and shot peening on fatigue striations during FCGR study of Ti6Al4V [J]. International Journal of Fatigue, 2016, 93: 38−50.

[18] HASSANI-GANGARAJ S M, CHO K S, VOIGT H J L, GUAGLIANO M, SCHUH C A. Experimental assessment and simulation of surface nanocrystallization by severe shot peening [J]. Acta Materialia, 2015, 97: 105−115.

[19] LIU Y G, LI M Q, LIU H J. Surface nanocrystallization and gradient structure developed in the bulk TC4 alloy processed by shot peening [J]. Journal of Alloys and Compounds, 2016, 685: 186−193.

[20] CHURCHMAN A T. The slip modes of titanium and the effect of purity on their occurrence during tensile deformation of single crystals [J]. Mathematical and Physical Sciences, 1997, 226: 216−226.

[21] SALEM A A, KALIDINDI S R, DOHERTY R D. Strain hardening of titanium: Role of deformation twinning [J]. Acta Materialia, 2003, 51: 4225−4237.

[22] WEN Ming, LIU Gang, GU Jian-feng, GUAN Wei-ming, LU Jian. Dislocation evolution in titanium during surface severe plastic deformation [J]. Applied Surface Science, 2009, 255: 6097−6102.

[23] BHATTACHARYYA D, CERRETA E K, MCCABE R, NIEWCZAS M, GRAY G T, MISRA A, TOMÉ C N. Origin of dislocations within tensile and compressive twins in pure textured Zr [J]. Acta Materialia, 2009, 57: 305−315.

[24] LIU X C, ZHANG H W, LU K. Formation of nano-laminated structure in nickel by means of surface mechanical grinding treatment [J]. Acta Materialia, 2015, 96: 24−36.

[25] DYAKONOV G S, MIRONOV S, SEMENOVA I P, VALIEV R Z, SEMIATIN S L. EBSD analysis of grain-refinement mechanisms operating during equal-channel angular pressing of commercial-purity titanium [J]. Acta Materialia, 2019, 173: 174−183.

[26] LIU Y G, LI M Q. Structure response characteristics and surface nanocrystallization mechanism of alpha phase in Ti−6Al−4V subjected to high energy shot peening [J]. Journal of Alloys and Compounds, 2019, 773: 860−871.

[27] WU Ji-zhan, LIU Huai-ju, WEI Pei-tang, LIN Qin-jie, ZHOU Shuang-shuang. Effect of shot peening coverage on residual stress and surface roughness of 18CrNiMo7-6 steel [J]. International Journal of Mechanical Sciences, 2020, 183: 105785.

[28] KIM J C, CHEONG S K, NOGUCHI H. Evolution of residual stress redistribution associated with localized surface microcracking in shot-peened medium-carbon steel during fatigue test [J]. International Journal of Fatigue, 2013, 55: 147−157.

[29] PARIS P, ERDOGAN F. A critical analysis of crack propagation laws [J]. Journal of Basic Engineering, 1963, 85: 528−533.

[30] SUN Ru-jian, LI Liu-he, GUO Wei, PENG Peng, ZHAI Tong-guang, CHE Zhi-gang, LI Bo, GUO Chao, ZHU Ying. Laser shock peening induced fatigue crack retardation in Ti-17 titanium alloy [J]. Materials Science and Engineering A, 2018, 737: 94−104.

[31] ANDREWS S, SEHITOGLU H. A computer model for fatigue crack growth from rough surfaces [J]. International Journal of Fatigue, 2000, 22: 619−630.

[32] YODER G R, COOLEY L A, CROOKER T W. Quantitative analysis of microstructural effects on fatigue crack growth in Widmanstätten Ti−6A1−4V and Ti−8Al− 1Mo−1V [J]. Engineering Fracture Mechanics, 1979, 11: 805−816.

[33] LAN Liang, JIN Xin-yuan, GAO Shuang, HE Bo, RONG Yon-ghua. Microstructural evolution and stress state related to mechanical properties of electron beam melted Ti−6Al−4V alloy modified by laser shock peening [J]. Journal of Materials Science & Technology, 2020, 50: 153−161.

[34] ZABEEN S, PREUSS M, WITHERS P J. Evolution of a laser shock peened residual stress field locally with foreign object damage and subsequent fatigue crack growth [J]. Acta Materialia, 2015, 83: 216−226.

[35] YANG Mu-xin, PAN Yue, YUAN Fu-ping, ZHU Yun-tian, WU Xiao-lei. Back stress strengthening and strain hardening

in gradient structure [J]. Materials Research Letters, 2016, 4: 145−151.
[36] SUN Ru-jian, KELLER S, ZHU Ying, GUO Wei, KASHAEV N, KLUSEMANN B. Experimental-numerical study of laser-shock-peening-induced retardation of fatigue crack propagation in Ti-17 titanium alloy [J]. International Journal of Fatigue, 2021, 145: 106081.
[37] AGUADO-MONTERO S, VÁZQUEZ J, NAVARRO C, DOMíNGUEZ J. Optimal shot peening residual stress profile for fatigue [J]. Theoretical and Applied Fracture Mechanics, 2021, 116: 103109.
[38] ELBER. Fatigue crack closure under cyclic tension [J]. Engineering Fracture Mechanics, 1970, 2: 37−45.
[39] LI Yong, LIU Zhi-yong, FAN En-dian, CUI Zhong-yu, ZHAO Jin-bin. The effect of crack tip environment on crack growth behaviour of a low alloy steel at cathodic potentials in artificial seawater [J]. Journal of Materials Science & Technology, 2020, 54: 119−131.
[40] LI Jing, SUN Qiang, ZHANG Zhong-ping, LI Chun-wang, QIAO Yan-jiang. Theoretical estimation to the cyclic yield strength and fatigue limit for alloy steels [J]. Mechanics Research Communications, 2009, 36: 316−321.
[41] OULD C B, IMAD A, BENGUEDIAB M. Influence of the cyclic plastic zone size on the propagation of the fatigue crack in case of 12NC6 steel [J]. Computational Materials Science, 2008, 43: 1010−1017.
[42] CHEN Liang-bin, CAO Ting-hui, WEI Ran, TANG Ke, XIN Chao, JIANG Feng, SUN Jun. Gradient structure design to strengthen carbon interstitial $Fe_{40}Mn_{40}Co_{10}Cr_{10}$ high entropy alloys [J]. Materials Science and Engineering A, 2020, 772: 138661.
[43] WU X L, YANG M X, YUAN F P, WU G L, WEI Y J, HUANG X X, ZHU Y T. Heterogeneous lamella structure unites ultrafine-grain strength with coarse-grain ductility [J]. Proceedings of the National Academy of Sciences, 2015, 112: 14501-5.
[44] LIU Xiao-long, YUAN Fu-ping, ZHU Yun-tian, WU Xiao-lei. Extraordinary Bauschinger effect in gradient structured copper [J]. Scripta Materialia, 2018, 150: 57−60.
[45] LI Xiao, SUN Bin-han, GUAN Bo, JIA Yun-fei, GONG Cong-yang, ZHANG Xian-cheng, TU Shan-tung. Elucidating the effect of gradient structure on strengthening mechanisms and fatigue behavior of pure titanium [J]. International Journal of Fatigue, 2021, 146: 106142.

高能喷丸制备具有表面梯度结构的 Ti−6Al−4V 合金的疲劳裂纹扩展行为

朱文光，马 驰，张聪惠，胡 坤，曾祥康

西安建筑科技大学 冶金工程学院，西安 710055

摘 要：通过高能喷丸(HESP)在 Ti−6Al−4V 合金表面成功制备梯度结构，并研究其对疲劳裂纹扩展的影响。采用光学显微镜、扫描电子显微镜、透射电子显微镜和 X 射线衍射仪对 HESP 过程中的显微组织和残余应力演变进行表征。结果表明，材料表面形成的梯度纳米结构具有 220 μm 深度的残余压应力层。梯度纳米结构的产生能改善合金的强塑性匹配。最大残余压应力产生于次表层，且随着喷丸时间的增加逐渐增大。HESP 处理有效降低裂纹扩展速率，提高疲劳裂纹扩展寿命。残余压应力可降低裂纹尖端的有效应力强度因子范围($\Delta K'_{\mathrm{eff}}$)，从而产生裂纹闭合效应并延缓裂纹扩展。同时，晶粒细化引起的晶界增加、有效滑移长度减小和裂纹尖端塑性区的协同作用也会使裂纹扩展阻力增大。

关键词：Ti−6Al−4V 合金；高能喷丸；表面梯度结构；裂纹扩展速率

(Edited by Bing YANG)